

1 **Effects of Disturbance on Seasonal CO₂ Dynamics in Two Boreal Forest Sites**
2 **Underlain by Permafrost**~~Effects of permafrost thaw on seasonal soil CO₂~~
3 ~~efflux dynamics in a boreal forest site~~

Formatted: Subscript

4 Dragos A. Vas¹, Jaimie R. West², David Brodylo¹, Amanda J. Barker¹, ~~William Brad~~ Baxter¹,
5 and Robyn A. Barbato²

6 ¹ U.S. Army Engineer Research and Development Center-Cold Regions Research and Engineering
7 Laboratory, Ft. Wainwright, Alaska 99703, United States.

8 ² U.S. Army Engineer Research and Development Center-Cold Regions Research and Engineering
9 Laboratory, Hanover, New Hampshire 03755, United State.

10 Correspondence to Dragos Vas (Dragos.A.Vas@usace.army.mil) ORCID: 0009-0005-2319-5079.

11 **Abstract.** Permafrost regions in subarctic and arctic areas harbor substantial carbon reserves, which are
12 becoming increasingly vulnerable to microbial decomposition as soils warm. As the seasonally thawed
13 active layer deepens and anthropogenic disturbances escalate, accurately predicting carbon fluxes from
14 ~~disturbed~~thawed environments underlain by permafrost requires a comprehensive understanding of soil
15 respiration dynamics. This study ~~aimed to~~ investigated the impact of ~~surface~~ disturbance on ~~year-~~
16 ~~round~~seasonal soil ~~respiration rates~~biological properties in a boreal forest ecosystem near Fairbanks,
17 Alaska. Further, we sought to~~and~~ identify the key environmental and geochemical factors influencing
18 ~~these processes~~soil biology in the undisturbed and disturbed soils ~~in a boreal forest ecosystem near~~
19 Fairbanks, Alaska. Our results revealed a substantial rise in soil respiration at the disturbed boreal forest
20 site, which exhibited a 14.4% overall increase in CO₂ efflux compared to the undisturbed site. This effect
21 was most pronounced during the summer, when the increase in CO₂ efflux peaked at 20%. This
22 heightened respiratory activity was directly linked to significantly warmer soil conditions, with the mean
23 annual soil temperature at the disturbed site measuring $0.60 \pm 0.16^\circ\text{C}$, in stark contrast to the sub-zero
24 temperatures of $-0.37 \pm 0.08^\circ\text{C}$ at the undisturbed site~~The disturbed site demonstrated an increase in mean~~
25 ~~annual soil temperatures, recorded at $0.60 \pm 0.16^\circ\text{C}$, along with a 14.4% rise in mean annual microbial~~
26 ~~activity, which peaked at 20% during the summer, in contrast to the undisturbed site, which had a mean~~
27 ~~annual temperature of $-0.37 \pm 0.08^\circ\text{C}$. Furthermore, bacterial and fungal community composition differed~~
28 ~~significantly between the two sites, suggesting a potential mechanism underlying the variation in CO₂~~
29 ~~efflux. Furthermore, the disturbed site had 30% higher bacterial community richness, 1% higher total~~
30 ~~mean C and 0.03% higher total mean N concentration levels, and 11.9% higher pH values in the subsoil~~
31 ~~layer, as well as a 147% deeper maximum active thaw depth, suggesting potential controls underlying the~~
32 ~~variation in CO₂ efflux. Our research underscores the essential importance of considering the rise in~~
33 carbon emissions from anthropogenically disturbed soils ~~in disturbed areas underlain by~~ permafrost ~~areas,~~
34 which are frequently neglected in assessments of the carbon cycle. This study contributes to a deeper

Formatted: Subscript

Formatted: Subscript

Formatted: Subscript

35 understanding of the complex interactions governing soil respiration in [disturbed](#) permafrost
36 [environments](#), ultimately informing more accurate predictions of carbon fluxes in these ecosystems.

37 1. Introduction

38 Soil respiration, the process by which carbon dioxide (CO₂) is released from the soil surface to
39 the atmosphere, is a critical component of the global carbon cycle. This process
40 [encompasses](#) the microbial breakdown of organic material as well as the respiration of plant roots.
41 Understanding soil respiration dynamics is particularly crucial in boreal forests, as they
42 [comprise](#) approximately 30% of global forested area and play a vital role in global carbon
43 sequestration (Bonan, 2008; Pan *et al.*, 2011; Chi *et al.*, 2021). Recent studies indicate that increasing
44 temperatures could lead to boreal forests transitioning from functioning as carbon sinks to becoming
45 carbon sources (Bond-Lamberty *et al.*, 2018; Marty *et al.*, 2019; Harel *et al.*, 2023). In boreal forests, soil
46 respiration is estimated to contribute up to 68% of the total ecosystem respiration (Parker *et al.*, 2020;
47 Watts *et al.*, 2021) and is significantly impacted by changes in soil temperature, soil moisture, the
48 microbial community, and [vegetation type](#) (Grace, 2004; Fekete *et al.*, 2014;
49 Rodtassana *et al.*, 2021). Soil respiration in permafrost regions is also influenced by the
50 [thickening](#) of the active layer ([the seasonally thawed soil surface layer](#)) that occurs
51 [when permafrost is degraded due to](#) warmer temperatures
52 ([Koster et al., 2017](#); Turetsky *et al.*, 2020; Watts *et al.*, 2021).

53 [Anthropogenic \(e.g., trail development, firewood harvesting\) and natural \(e.g., wildfires, insects](#)
54 [and pathogens\) disturbances fundamentally alter the landscape and soil properties, which in turn governs](#)
55 [soil respiration and the stability of massive permafrost carbon stores \(Schepaschenko et al.,](#)
56 [2025; Miner et al., 2022\). The primary disturbance agents—fire, timber harvesting, and insect](#)
57 [outbreaks—have intensified, impacting millions of hectares annually \(Schepaschenko et al., 2025\).](#)
58 [Wildfires are the dominant natural disturbance in boreal forests, and their frequency and scale have grown](#)
59 [significantly in the recent years \(Zhu et al., 2022; Schepaschenko et al., 2025\). An intensified heat](#)
60 [flux can thicken the active layer \(Yoshikawa et al., 2002; Koster et al., 2017 and 20187; Zhu et al., 2022\)](#)
61 [to the point where it no longer refreezes completely in the winter, leading to the formation of a talik, or a](#)
62 [year-round unfrozen layer of soil above the permafrost, making carbon available to microorganisms year](#)
63 [round \(Yoshikawa et al., 2002; Zhu et al., 2022\).](#)

64

65

66
67
68
69
70
71
72
73
74
75
76
77
78
79
80
81
82
83
84
85
86
87
88
89
90
91
92
93
94
95
96
97
98

Anthropogenic disturbances in boreal forests alter carbon cycling through distinct short- and long-term phases that are primarily driven by impacts to the underlying permafrost. Initially, disturbances like forest harvesting can cause a temporary decrease in total soil CO₂ efflux by eliminating root (autotrophic) respiration (Akande et al., 2023; Schepaschenko et al., 2025). However, this short-term effect is overshadowed by the dominant, long-term consequences of physical changes to the ground's thermal regime. Activities such as land clearing for infrastructure and resource exploration remove the insulating vegetation and surface organic layers, leading to warmer soil temperatures and a deeper active layer (Forbes et al., 2002; Foster et al., 2022). This permafrost degradation exposes vast stores of previously frozen organic carbon to microbial decomposition, transforming the disturbed landscape into a persistent, long-term source of atmospheric CO₂ (Koster et al., 2018; Miner et al., 2022). As ecosystems recover, the combination of this sustained decomposition with new root respiration can lead to total soil efflux rates that ultimately exceed those of undisturbed forests (Akande et al., 2023). Consequently, these human disturbances are a critical factor that accelerates the permafrost carbon feedback, significantly impacting the overall carbon balance of the circumpolar north (Schepaschenko et al., 2025; Miner et al., 2022).

Despite their importance, the cumulative impacts of these anthropogenic disturbances on landscape and soil properties are not well understood, often being overshadowed by the more extensively studied effects of wildfire (Foster et al., 2022). Therefore, investigating soil respiration in disturbed, permafrost-affected environments is crucial for assessing the resilience and vulnerability of boreal ecosystems.
Under projected climate scenarios, the frequency and intensity of disturbances in these regions are expected to increase, potentially leading to significant changes in soil carbon fluxes (Schepaschenko et al., 2025).

Further, insights gained from such studies can inform forest management practices aimed at mitigating the impacts of disturbances and preserving the carbon sequestration potential of boreal forests.

99
100
101
102
103
104
105
106
107
108
109
110
111
112
113
114
115
116
117
118
119
120
121
122
123
124
125
126
127
128
129
130
131

The aim of this study is to measure and compare the soil respiration rates in undisturbed and disturbed sites in a subarctic boreal forest. The disturbance was due to historical activities related to mining such as trail development and firewood harvest. These disturbances took place in the early 1920s, coinciding with the construction of a drainage ditch and an access trail to support mining operations in the area. During the trail and draining ditch development the groundcover vegetations and surface soils were disturbed, and the trees were harvested. Currently, there is no active drainage at the research site, and the trail is seldom used. We hypothesize that the disturbance had a lasting effect on soil activity and properties and there will be a significant difference in the measurements between the undisturbed and disturbed sites. Further, we hypothesize that this trend also occurs in winter, where measurements are severely lacking, though soils are active.

To reveal the fundamental controls driving variation in soil respiration within and between the disturbed and undisturbed boreal forest sites, we examined seasonal soil CO₂ efflux alongside various edaphic factors, including soil temperature, moisture content, soil organic matter (SOM), pH, and the composition of microbial communities. To assess this relationship, a non-linear Random Forest Model (RFM) was used in conjunction with regression analysis to analyze the time series data, which encompassed variables such as soil respiration, temperature, moisture, and air temperature. Additionally, R statistical ANOVA analysis was performed to evaluate soil characteristics, particularly pH and SOM, as well as the composition of soil microbial communities. The emissions data and estimates of carbon fluxes will be helpful to improve carbon modeling efforts. In the following sections, we detail the study site and our methodological approach (Section 2), present the key findings related to soil conditions and respiration (Section 3), and discuss the implications of these findings for understanding carbon cycling in disturbed permafrost ecosystems (Section 4).

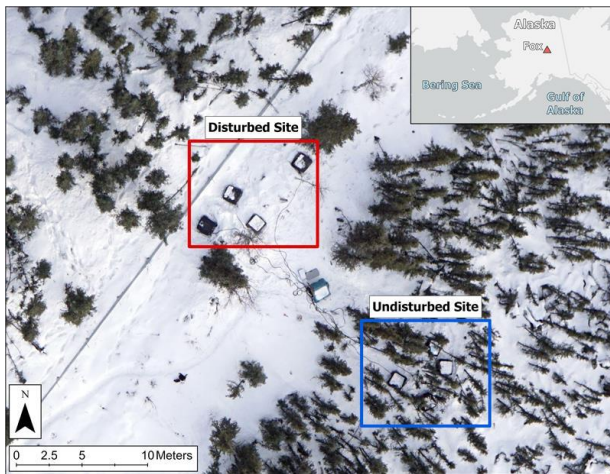
Formatted: Subscript

132 **2. Materials and Methods**

133 **2.1 Site description**

134 The study was conducted at two adjacent sites underlain by permafrost in a
135 subarctic boreal forest, of the discontinuous permafrost region, located at the U.S. Army Cold Regions
136 Research and Engineering Laboratory (CRREL) Permafrost Research Tunnel Facility in Fox, Alaska
137 (64.9507 N -147.6200 W, 248 m a.s.l.). The region experiences a continental climate, which is defined by
138 an average annual air temperature of $-2.4\text{ }^{\circ}\text{C}$, with average temperatures in July reaching $16\text{ }^{\circ}\text{C}$ and
139 January temperatures averaging $-21.9\text{ }^{\circ}\text{C}$; extreme temperatures throughout the year can range from
140 $-51\text{ }^{\circ}\text{C}$ to $38\text{ }^{\circ}\text{C}$ (Jorgenson et al. 2020). The two sites were situated approximately 10 m apart, (Figure 1)
141 and exhibited comparable topography and parent material. The first site consists of an undisturbed black
142 spruce forest ecosystem (SI Figure S1); the second consists of an anthropogenically disturbed area where
143 trails were established, and black spruce tree cover was removed in firewood harvests
144 during mining activities in the region in the 1920's.

Formatted: Font: (Default) Times New Roman



145
146 **Figure 1.** Aerial view of the study sites and experimental setup. The image displays the geographical
147 location and the layout of the sample plots at the undisturbed (blue rectangle) and disturbed (red
148 rectangle) study sites. The aerial image was captured on March 18, 2023. (Image credit: Dr. David
149 Brodylo).

150 The vegetation at the undisturbed site consists of small black spruce (*Picea mariana*) ranging
151 from densely distributed to tightly spaced. Understory canopy is dominated by marsh and bog Labrador
152 tea (*Rhododendron tomentosum*; *groenlandicum*). Forest floor cover is primarily mosses (*i.e.*, feather

Formatted: Font: Italic

153 mosses and *Sphagnum spp.*) and small shrubs including lowbush cranberry (*Vaccinium vitis-idaea*). The
154 disturbed site is characterized by scattered birch (*Betula neolaskana*) and tall black spruce (*Picea*
155 *mariana*) cover. The understory canopy is primarily dwarf shrubs including marsh Labrador tea
156 and bog blueberry (*Vaccinium uliginosum*). The ground surface cover is dominated by grasses (*Poaceae*)
157 and sedges (*Cyperaceae*). The typical undisturbed soil profile at this site consists of a fibric organic layer
158 of variable thickness, which primarily contains undecayed and partially decayed moss and forest litter
159 materials (O horizon), underlain by an organic-rich mineral material layer containing hemic-sapric
160 organic fraction (A/B horizon), and thick accumulations of mineral material at the base (B/C horizon).
161 Disturbance seemingly impacts the thickness of the surface organic layer. Soil sampling at each site
162 targeted soil materials below the organic horizon. The sampled soil material at the two sites were
163 classified as mineral soil material (<20% organic matter [OM]; Soil Survey Staff, 2022) with a
164 subdivision of more organic-rich fractions (10-18% OM) comprising a “topsoil” layer
165 (akin to an A horizon) that starts below the organic layer (O horizon), and more mineral-rich
166 material (<5% OM) comprising a “subsoil” layer.
167 The topsoil textures ranged from loam to silt loam, reflecting a higher proportion of sand particles in the
168 topsoil relative to the silt loam-textured subsoil (SI Table 1).

169 **2.2. Installation of soil and meteorological sensors**

170 Four plots were established at an undisturbed site, and the other four were located at an adjacent
171 disturbed site (Figure 1). At each site, sensors were distributed to measure total soil respiration
172 (autotrophic and heterotrophic), temperature, and volumetric water content (VWC) every
173 30 minutes from November 4, 2022, to November 9, 2023. During the same period, air temperature and
174 barometric pressure were recorded every 15 minutes. Because some of the sensors have robotic arms to
175 collect measurements that would be impeded by snowfall in the winter, Costco folding tables (Columbus,
176 Indiana) with a surface of 91.4 cm × 91.4 cm were situated above the plots, during that
177 period, to prevent snow accumulation (Figure 2b). The folding tables were removed at the onset of
178 the snow-free season to reduce interference with natural environmental factors such as rain and solar
179 radiation (Figure 2c).

180 Soil temperature, VWC, air temperature, and barometric pressure were measured using the
181 following Onset HOBO (Onset, Bourne, Massachusetts, USA) instrumentation: U30 USB Weather
182 Station, S-TMB-M002 12-Bit Temperature Smart Sensor, S-SMC-M005 EC5 Soil Moisture Smart
183 Sensor, S-THC-M002 Temperature/Relative Humidity Smart Sensor, and S-BPB-CM50 Smart
184 Barometric Pressure Sensor. Soil temperature and VWC were recorded in the topsoil and subsoil layers,

185 approximately 30 cm from each soil respiration sensor, at a depth of 18.5 ± 1.19 cm in the topsoil layer
186 and 34.5 ± 1.47 cm in the subsoil layer for the undisturbed site. At the disturbed site, the measurements
187 were taken at 13.5 ± 2.53 cm in the topsoil layer and 35.5 ± 1.85 cm in the subsoil layer. These depths
188 were measured from the top of the ground vegetation cover (the moss surface). At both sites, the
189 temperature and VWC sensors of the topsoil were installed below the fibric organic layer that had a
190 thickness of 16.5 ± 1.19 cm at the undisturbed site and 9.5 ± 0.87 cm at the disturbed site. The differences
191 in sensor placement depth were influenced by the variations in the thickness of the organic layer between
192 the two sites (SI Figure S2). VWC measurements were restricted to the summer and autumn seasons due
193 to the sensor's inability to measure below freezing temperatures. Air temperature and barometric pressure
194 were measured at 2 m above the substrate surface.

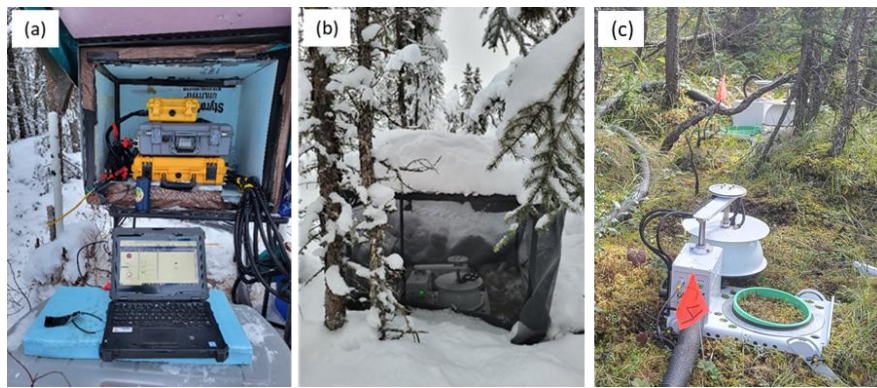
195 The depth of thaw in the active layer was assessed at ~ 10 cm from each of the eight chamber
196 plots during each site visit ($n = 160$) from 12 May to 3 Oct 2023. To determine this depth, a graduated
197 metal rod with a diameter of 1 cm (known as a frost probe) was inserted into the ground, at the same
198 location, until it met resistance, establishing the distance between the ground surface vegetation and the
199 top of the frozen soils (Shiklomanov *et al.* 2013).

200 For the soil respiration measurements, which encompasses the overall release of CO_2 from the
201 soil into the atmosphere (including both autotrophic and heterotrophic processes), we installed 21.3 cm
202 diameter thick-walled polyvinyl chloride (PVC) collars (LI-COR inc., Lincoln, Nebraska, USA) in the
203 center of each plot. They were a height of 11.4 cm and were inserted 2-3 cm into the soil through the soil
204 vegetation cover. The collars spacing varied from two to four meters at the undisturbed site and from
205 three to eight meters at the disturbed site. (Figure 1). We installed a 8200-104 Opaque Long-Term
206 Chamber (LI-COR inc., Lincoln, Nebraska, USA) above each collar, which yielded a total of eight. The
207 chambers were connected via 15 m long tubing and cable assembly to a LI-8250 multiplexer (LI-COR
208 inc., Lincoln, Nebraska, USA) that linked to a LI-870 $\text{CO}_2/\text{H}_2\text{O}$ gas analyzer (LI-COR inc., Lincoln,
209 Nebraska, USA). The cable and tubing assembly was wrapped in 1.3 cm thick tubular pipe insulation
210 foam to prevent internal clogging from freezing moisture to ensure data collection in winter.

211 **2.3 Respiration Data Collection**

212 The measurement process followed a closed-chamber dynamic methodology, which was
213 automated and controlled by the LI-8250 Multiplexer. At 30 minute intervals, the multiplexer would
214 initiate a measurement at one of the chamber locations. This involved the 8200-104 chamber
215 automatically rotating and lowering to seal onto the pre-installed PVC soil collar, creating a closed
216 headspace over the soil surface. Once the chamber was sealed, the LI-8250 directed a closed loop of air

217 from the chamber headspace to the LI-870 and LI-7810 analyzers and back. The gas analyzers measured
218 CO₂ and H₂O concentrations, for a period of 120 seconds, at a rate of 1 Hz. As CO₂ was respired
219 , its concentration within the closed system increased over time. The soil CO₂ flux was calculated
220 from the rate of this concentration increase. After each measurement cycle, the chamber automatically
221 opened, and the system proceeded to the next chamber in the sequence. A more detailed description of the
222 soil gas flux system's operation and these winter modifications can be found in Vas et al. (2023).
223 Throughout the year, we performed site visits on a near-weekly basis to download data and maintain the
224 equipment. Standard maintenance involved visually inspecting each chamber and clearing the seals of any
225 debris. During winter months, this was supplemented by ensuring the protective tables remained free of
226 deep snow, a necessary step to allow for sufficient air exchange to ensure the accuracy of the
227 measurements.



228
229 **Figure 2.** Custom modifications for LI-COR Soil gas flux system in cold climates.
230 Enclosures were designed to ensure optimal operating temperatures (a) (photo credits: Dragos A. Vas, 17
231 November 2023), insulated tubing for instruments to prevent clogging, and long-term covers for
232 chambers (b) (photo credits: Dragos A. Vas, 13 January 2023) to inhibit snow accumulation or
233 drifting on the chambers. Snow free season photo of the chamber (c) (photo credits: Dragos A. Vas, 13
234 August 2023); the long-term covers were removed at the beginning of the snow free season.

Formatted: Font: Not Bold

Formatted: Font: Not Bold

Formatted: Font: Not Bold

Formatted: Font color: Text 1

Formatted: Font: Not Bold

235 2.5 Soil collection and property analysis

236 Soil samples were collected from both the topsoil and subsoil layers across all plots in the autumn
237 (September 2022), winter (February 2023), and summer (June 2023) seasons to analyze potential
238 variations in microbial community composition among seasons, disturbance regimes, and soil layers. The
239 samples were collected at identical depths during each season, which coincided with the depth at which
240 the soil temperature and moisture probes were positioned; these depths varied for each plot according to

241 [the organic layer thickness](#). The winter samples were acquired using a gas-powered SIPRE (Snow, Ice,
242 and [Permafrost Research Establishment](#)) corer (Jon's Machine Shop, Fairbanks, Alaska, USA). Nitrile
243 gloves were utilized to minimize any potential contamination to the cores. Furthermore, the SIPRE corer
244 and all associated tools were thoroughly sanitized with 70% isopropyl alcohol, DNA away, and RNase
245 away (Thermo Fisher Scientific in Waltham, MA, USA). The cores were then subsampled into
246 approximately 5 cm long cylinders using a sanitized hammer and chisel and were carefully placed into
247 sterile Nasco™ Whirl-pak bags (Thermo Fisher Scientific, Waltham, MA, USA); further information on
248 this sampling method can be found in [Barbato *et al.* \(2022\)](#). Summer and autumn soil samples were
249 gathered using a sanitized trowel with 70% isopropyl alcohol, DNA away, and RNase away. The samples,
250 approximately 5 cm thick, were placed in sterile Nasco™ Whirl-pak bags and immediately placed in a
251 cooler with frozen ice packs, then transferred to a freezer upon arrival at the Cold Regions Research and
252 Engineering Laboratory in Fairbanks, Alaska (CRREL-AK). All collected soil samples were kept at a
253 temperature of -25 °C until shipped to CRREL in Hanover, New Hampshire (CRREL-NH), where they
254 were stored at -20 °C until further processing. [Deep freezing the soil samples immediately after collection
255 and maintaining this state until processing halts microbial growth and facilitates the preservation of the
256 microbial community structure at the moment of sampling \(Baker *et al.*, 2023; Doherty *et al.*, 2020\).](#)

257 Loss on ignition (LOI) was measured as a proxy for SOM content (Storer,
258 1984) on all soil samples. Here, LOI is the proportion of mass loss from oven-dried soil (dried at 105 °C
259 for 24 hours) following 2 hours at 360 °C in a muffle furnace. Soil total carbon and total nitrogen was
260 measured via combustion using a TruSpec C and N Analyzer (LECO, St. Joseph, MI, USA) at the
261 University of Wisconsin Soil and Forage Lab. Soil pH was measured from a 1:1 slurry of soil:CaCl₂
262 solution (0.01M) using a pH probe (Hanna Instruments, Woonsocket, RI, USA) and a SevenEasy S20 pH
263 meter (Mettler Toledo, Columbus, OH, USA). Soil pH was converted to H⁺ concentration prior to taking
264 an average or statistical analysis. LOI total carbon, total nitrogen and soil pH [were](#) statistically
265 analyzed using ANOVA in R.

266 **2.6 Soil microbial DNA extraction, gene sequencing, and data analysis**

267 Soil was partially defrosted and homogenized in the sample bag prior to subsampling 250 mg into
268 bead beating tubes. Total genomic DNA was extracted using the DNeasy PowerSoil Pro Kit (Catalog No.
269 47014, Qiagen, Germantown, MD, USA), using a Precellys Evolution Touch homogenizer for the bead
270 beating step (Catalog number P002511-PEVT0-A.0, Bertin Technologies, Montigny-le-Bretonneux,
271 France). Automated DNA extraction was done with a QIAcube Connect (Catalog No. 9002864, Qiagen,
272 Germantown, MD, USA) and each extraction run included a blank. Extracted DNA was held at -20 °C.

Formatted: Font color: Text 1

Formatted: Font color: Text 1

273 Library preparation and sequencing was completed at Argonne National Laboratory (Lemont, IL,
274 USA), as follows. For bacterial analysis, the V4 region of the 16S rRNA gene was targeted for PCR
275 amplification with region-specific primers (forward primer 515F and reverse primer 806R); and for
276 fungal analysis, the ITS region was amplified using appropriate barcoded primers (Caporaso *et al.*, 2011;
277 Caporaso *et al.*, 2012; Apprill *et al.*, 2015; Parada *et al.*, 2016; Smith *et al.*, 2014; Walters *et al.*, 2016).
278 Each PCR reaction contained 1 μ L template DNA, 12.5 μ L AccuStart II PCR ToughMix (Quantabio,
279 Beverly, MA, USA), 1 μ L forward primer with Golay barcode (5 μ M concentration), 1 μ L reverse primer
280 (5 μ M concentration), and 9.5 μ L DNA-free PCR water. PCR conditions were: 94 $^{\circ}$ C (3 minutes to
281 denature the DNA); 35 cycles of 94 $^{\circ}$ C (45 s), 50 $^{\circ}$ C (60 s), and 72 $^{\circ}$ C (90 s); final extension at 72 $^{\circ}$ C (10
282 minutes). PCR product was quantified using Quant-iT PicoGreen (P7589, Invitrogen, Waltham, MA,
283 USA). Equimolar amounts of amplicons were pooled, purified using AMPure XP Beads (A63881,
284 Beckman Coulter, Brea, CA, USA), quantified (Qubit, Invitrogen), and diluted to 6.75 pM using a 10%
285 PhiX spike. Paired-end 2 x 251 sequencing was done on a MiSeq (Illumina, San Diego, CA, USA).

286 Sequencing data were processed in R (R-Core-Team, 2018), using a dada2 v1.18.0 pipeline
287 (Callahan *et al.*, 2016), as in Baker *et al.* (2023), implemented using Snakemake v7.25.0 (Mölder *et al.*,
288 2021). Taxonomy assignment was based on the SILVA 138.1 reference database for 16S sequences (Quast
289 *et al.*, 2013; Yilmaz *et al.*, 2013) and the UNITE database (release 25.07.2023) for ITS sequences (Köljalg
290 *et al.*, 2013; Nilsson *et al.*, 2019). Chloroplasts and mitochondria were excluded from the dataset. A total
291 of 2836 fungal ASVs and 10,608 bacterial ASVs were identified (excluding extraction blanks). Amplicon
292 sequences are in the National Center for Biotechnology Information Sequence Read Archive (NCBI
293 SRA), accession PRJNA1178745. Though our bacterial primers targeted both bacterial and archaeal 16S
294 rRNA, we will refer simply to bacteria, which comprise 99.8% of total reads. Of archeal reads, 80%
295 represented the phylum *Crenarchaeota*. One sample was excluded from analysis because it was
296 mislabeled (2023_Feb, Chamber 3, Organic).

297 R [software](#) (R-Core-Team, 2018), and *ggplot2* (Wickham, 2016) were used for data analysis and
298 visualization; the bioinformatic approach followed West *et al.* (2022). Community composition was
299 visualized using principal coordinates analysis (PCoA) of Bray-Curtis dissimilarities (Bray and Curtis,
300 1957) generated using *avgdist* from the R package *vegan* (Oksanen *et al.*, 2024) using rarefaction (999
301 iterations) to a sampling depth of 16,300 for 16S and 6150 for ITS. A significant effect ($p < 0.05$) of
302 disturbance, sampling date, and interaction of these factors on community composition was tested within
303 each soil layer (topsoil and subsoil), using permutational multivariate analysis of variance
304 (PERMANOVA; *adonis2* from *vegan*) (Anderson, 2001). Richness was evaluated using weighted linear
305 regression (*beta* function in *breakaway* R package) (Willis *et al.*, 2017), and a significant effect of

306 disturbance tested via ANOVA. Differential abundance (*differentialTest* in the *corncob* package) (Martin
307 *et al.*, 2021) was then used to identify significant enrichment or depletion of individual taxa due to
308 disturbance, after excluding taxa with mean relative abundance < 0.00001.

309 **2.7 Linear regression analysis**

310 For statistical analysis, data on soil respiration, soil temperature, and VWC, as well as air temperature and
311 barometric pressure from the eight chamber plots (four located at the disturbed site and four at the
312 undisturbed site), were averaged to obtain daily means (n=333 per variable) and seasonal means (n=4 per
313 variable). Seasons were defined according to observed efflux seasonality at the research site, a
314 classification consistent with previous research on boreal forest efflux (Wats *et al.*, 2021): winter
315 (November to March, n=123), spring (April to May, n=57), summer (June to August, n=92), and autumn
316 (September to October, n=61). Using these processed data, we performed a series of linear regression
317 analyses to determine the existence of distinct, linear trends between CO₂ efflux and each environmental
318 variable. This analysis was conducted separately for each site and season, and the coefficient of
319 determination (R²) was calculated to quantify the strength of each trend. Additionally, a one-way Analysis
320 of Variance (ANOVA) was used to test for statistically significant differences between the disturbed and
321 undisturbed sites. A p-value of less than 0.05 was considered significant for all tests. All statistical linear
322 regression analyses were conducted using Microsoft Excel.

323 **2.8 Random Forest modeling**

324 A regression-based Random Forest (RF) non-linear model developed in R was used to identify
325 the relative importance of the input variables to predict hourly and daily CO₂ concentrations. RF was
326 chosen over other algorithms due to its wide and successful application in determining variable
327 importance (Behnamian *et al.*, 2017; Lei *et al.*, 2024). In RF, the supervised non-linear algorithm can
328 combine predictions from hundreds or thousands of individual decision trees via bootstrap aggregation to
329 generate an ideal output (Schonlau and Zou, 2020). Compared with individual decision trees, this results
330 in an increase in generalization accuracy and a reduction in overfitting. A repeated k-fold cross-validation
331 technique was also employed. In this technique, data are randomly separated into *k* subsets with *k*-1 used
332 to train the model and the remainder to test the model, which is then repeated a specified amount. We
333 selected a value of 10 for *k* and a value of 5 for repetition. Input variables were the same for each instance
334 except barometric pressure being dropped for daily CO₂ concentrations due to poor importance values.
335 Thaw depth was static in the dataset that the model used from 4 October through 16 May due to the
336 presence of a frozen surface layer preventing thaw depth probing. Organic soil VWC and mineral soil

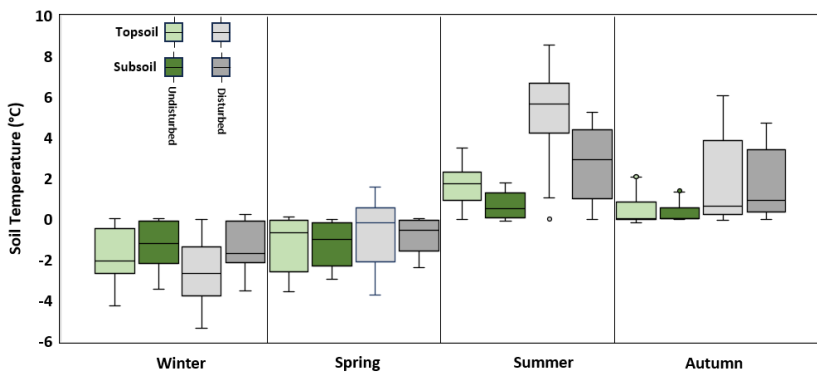
Formatted: Font: (Default) Times New Roman, Font color: Black, Pattern: Clear (White)

337 VWC from 1 November – 31 March and 1 April – 31 May were omitted for machine learning due to the
338 inability of the probes to function properly in subzero temperatures.

339 3. Results

340 3.1 Soil conditions

341 Soil temperature fluctuated by a factor of three at the disturbed site and by a factor of 1.9 at the
342 undisturbed site over the course of the year. The undisturbed and disturbed sites exhibited contrasting
343 thermal regimes. At the undisturbed site, the mean annual soil temperatures were below freezing,
344 exhibiting -0.33 ± 0.1 °C for topsoil and -0.41 ± 0.07 °C for subsoil (Figure 3). In contrast, the disturbed
345 site experienced positive mean annual soil temperatures, with 0.72 ± 0.2 °C for topsoil and 0.48 ± 0.13 °C
346 for subsoil. Winter was the only season with warmer topsoil and subsoil temperatures at the undisturbed
347 site. For both the undisturbed and disturbed sites, the subsoil layer was cooler than the topsoil layer in
348 terms of mean annual temperature. Significantly warmer soil temperatures were observed at the disturbed
349 site during the summer (4.04 ± 0.19 °C; $p < 0.001$, ANOVA) and autumn (1.88 ± 0.23 °C; $p < 0.001$,
350 ANOVA) in comparison to the temperatures recorded at the undisturbed site during the same seasons.
351 Conversely, the mean summer soil temperature at the undisturbed site was 1.15 ± 0.08 °C, while the mean
352 autumn soil temperature was 0.38 ± 0.07 °C (Figure 3). Soil temperatures in the shallower topsoil layer
353 exhibited greater variability throughout the year compared to the temperatures in the deeper subsoil layer
354 at both sites (Figure 3).

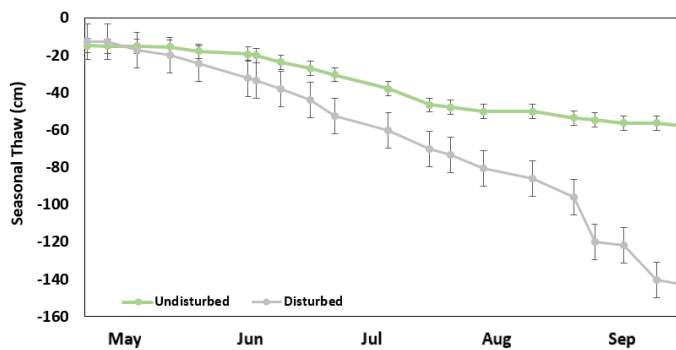


355 **Figure 3.** Seasonal soil temperature patterns. The seasons were delineated as winter (Nov–Mar), spring
356 (Apr and May), summer (Jun–Aug), and autumn (Sep and Oct). Soil temperature are average daily values
357 from the topsoil and subsoil layers at the 8 chamber plots: 4 at the undisturbed site and 4 at the disturbed
358 site. The range of the boxplot represents the first and third quartiles, while the central line signifies the
359

Formatted: Font: Not Bold

360 median. The whiskers of the box extend to the minimum and maximum values, with outliers represented
361 by circles.

362 VWC values ranged from $0.29 \pm 0.00 \text{ m}^3/\text{m}^3$ to $0.47 \pm 0.00 \text{ m}^3/\text{m}^3$ (1 Jun to 31 Oct 2024) (SI
363 Figure S3). Subsoil layer exhibited elevated mean seasonal VWC values, as compared to the topsoil
364 layer, at both locations (p values from 0.04 to < 0.001 , ANOVA). Average maximum seasonal thaw depth
365 exhibited significant differences between the two locations (p values 0.02, ANOVA), ranging from 58 ± 3
366 cm or 143 ± 29 cm at the undisturbed site or disturbed site, respectively (Figure 4). While the maximum
367 seasonal thaw depth remained relatively consistent across the undisturbed plots, ranging from 50 cm to 61
368 cm, the disturbed plot displayed a larger range in maximum thaw depth, varying from 82 cm to 204 cm.



369

370 **Figure 4.** Average seasonal thaw depth at the undisturbed and disturbed sites measured using manual
371 frost probe measurements from 12 May to 3 Oct 2023. Error bars are standard error.

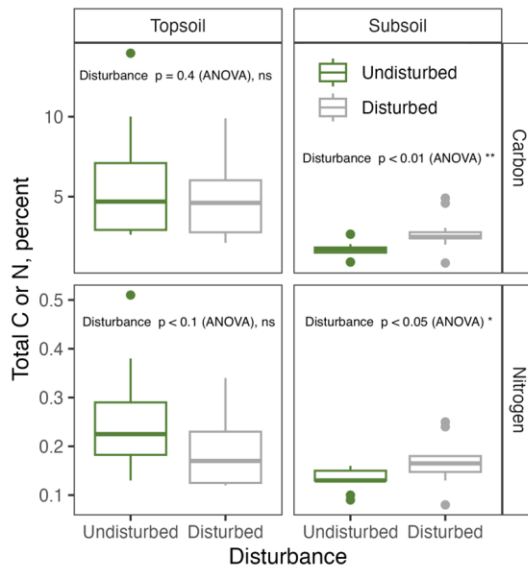
Formatted: Font: Not Bold

372 3.2 Soil properties

373 The disturbance had a significant effect on LOI (a proxy for SOM content) in the
374 subsoil layer, but not the topsoil layer (SI Figure S4). There was no significant effect of sampling date or
375 significant interaction of sampling date and disturbance on LOI. Mean total C concentration for
376 subsoil at the disturbed site was 2.7% (averaged across LiCor chamber plots and sampling
377 dates), significantly greater than that of the undisturbed site mean of 1.7% ($p < 0.01$; ANOVA).
378 Mean LOI for the topsoil layer was 0.122 and 0.142 for disturbed and undisturbed, respectively (not
379 significantly different).

380 Similarly, the disturbance was a significant factor for soil total C concentration and
381 total N concentration in the subsoil layer ($p < 0.01$ and $p < 0.05$, respectively; ANOVA), but not the
382 topsoil layer (Figure 5), and there was no significant effect of sampling date or significant interaction of

383 sampling date and disturbance on either C or N. Mean total C concentration for the topsoil layer was 4.7%
 384 and 5.8% for disturbed and undisturbed, respectively (not significantly different). Mean total N
 385 concentration for subsoil at the disturbed site was 0.16%, significantly greater than that of the
 386 undisturbed mean of 0.13% ($p < 0.01$; ANOVA). Mean total N concentration for the topsoil was 0.19%
 387 and 0.25% for disturbed and undisturbed, respectively (not significantly different).



388

389 **Figure 5.** Soil total carbon and total nitrogen, at the disturbed and undisturbed sites.
 390 Boxplots represent all three sampling dates and four LiCor chamber plots, within each
 391 site.

Formatted: Font: Not Bold

392 Similar to the response of LOI, total C, and total N, soil pH was significantly different in the
 393 subsoil layer, depending on the site; the effect of disturbance on the topsoil layer
 394 was not significant (SI Figure S5). There was no significant effect of sampling date or significant
 395 interaction of sampling date and disturbance on soil pH. Mean pH for subsoil in the disturbed
 396 site was 4.63 (averaged across chambers and sampling dates), significantly greater than that of
 397 the undisturbed site mean of 4.11 ($p < 0.01$; ANOVA). Mean pH for the topsoil layer was 3.78
 398 and 3.79 for disturbed and undisturbed, respectively (not significantly different).

Formatted: Font: (Default) Times New Roman

399 **3.3 Soil microbial community composition and diversity**

400 We compared microbial community composition and diversity between the disturbed and
 401 undisturbed sites to enhance our understanding of the role that microbes play in soil respiration. By
 402 examining the effects of the site disturbance on microbial diversity—quantified through variations in
 403 species richness and community structure—we can ascertain which microbial groups exhibit the greatest
 404 sensitivity to environmental alterations and how their functional roles might adapt in response.

405 The dominant bacterial phyla included *Proteobacteria*, *Acidobacteria*, *Actinobacteria*, *Verrucomicrobia*,
 406 The dominant bacterial phyla included *Proteobacteria*,
 407 *Acidobacteria*, *Actinobacteria*, *Verrucomicrobia*, and *Chloroflexi*, which together comprised over 75% of
 408 relative abundance (Figure 6). For fungi, 54% of relative abundance was comprised of *Ascomycota*
 409 (mostly classes *Leotiomycetes* and *Archaeorhizomycetes*), and 40% was *Basidiomycota* (mostly class
 410 *Agaricomycetes*) (Figure 6). Differential abundance testing only identified several dozen taxa (after
 411 filtering for somewhat higher abundance taxa) that were either significantly enriched or depleted under
 412 disturbance (see SI Figures S6 and S7). Notably, several Chloroflexi and Dormibacterota (a newly named
 413 phylum, previously identified as Chloroflexi) ASV's are depleted under disturbance relative to the
 414 undisturbed condition in subsoil, particularly at the February sampling date (SI Figure S7).



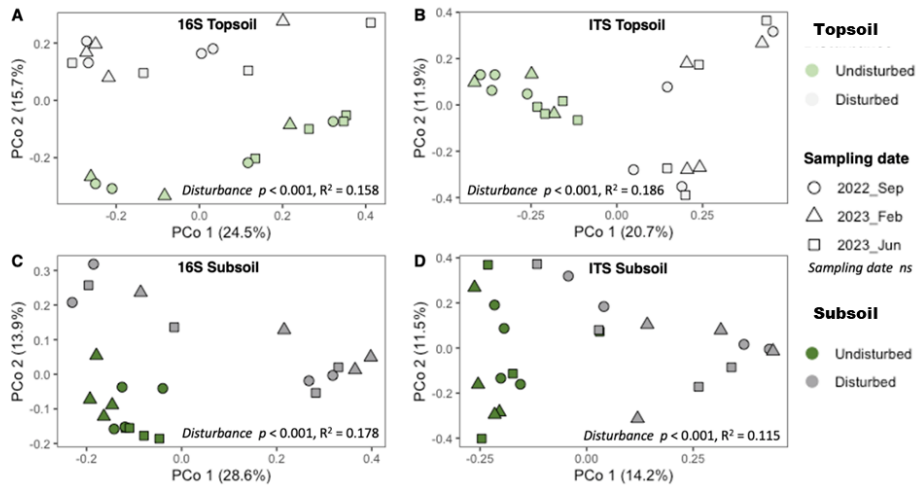
415
 416 **Figure 6.** Relative abundances of dominant bacterial phyla, faceted by sampling date and soil layer. Each
 417 plot is named for LiCor chamber (Ch1 through Ch8); Ch1, Ch2, Ch3, Ch4 are undisturbed plots, and Ch5,
 418 Ch6, Ch7, Ch8 are disturbed plots. One sample was excluded from analysis (2023_Feb, Chamber 3,
 419 Topsoil).



420
 421 **Figure 7.** Relative abundances of dominant fungal classes, faceted by sampling date and soil layer. Each
 422 plot is named for LiCor chamber (Ch1 through Ch8); Ch1, Ch2, Ch3, Ch4 are undisturbed plots, and Ch5,
 423 Ch6, Ch7, Ch8 are disturbed plots. One sample was excluded from analysis (2023_Feb, Chamber 3,
 424 Topsoil).

425 Mean estimated bacterial richness across the dataset was 711.5 ASVs, with a significant
 426 differences between the two sites (SI Figure S8). Overall, the disturbed samples had 30%
 427 higher richness compared to the undisturbed samples ($p < 0.01$, ANOVA); within each date and soil layer
 428 combination, only the February 2023 subsoil samples demonstrated a significant effect of disturbance (p
 429 < 0.01 , ANOVA). There was no effect of sampling date or soil layer, or interaction amongst the factors.
 430 Mean estimated fungal richness across the dataset was 165 ASVs; there was no effect of disturbance,
 431 sampling date, soil layer, or interaction amongst the factors (SI Figure S8).

432 Employing Bray-Curtis dissimilarities to assess beta diversity (Figure 8), we observed notable
 433 differences between the undisturbed and disturbed sites, concerning both bacterial and fungal
 434 communities in the topsoil and subsoil layers
 435 ($p < 0.001$ for all; $R^2 = 0.158, 0.178, 0.186, 0.115$ for bacterial topsoil, bacterial subsoil, fungal topsoil,
 436 ($p < 0.001$ for all; $R^2 = 0.158, 0.178, 0.186, 0.115$ for bacterial topsoil,
 437 bacterial subsoil, fungal topsoil, and fungal subsoil communities, respectively; PERMANOVA). Sampling
 438 date did not have a significant effect.



439

440 **Figure 8.** Principal coordinates analysis of Bray-Curtis dissimilarities of relative abundance data
 441 following rarefaction. Panels (A) and (C) represent the bacterial community (16S marker), and panels (B)
 442 and (D) represent the fungal community composition (ITS marker). The top panels (A & B; lighter
 443 shades) represent the topsoil layer community composition, while the bottom panels (C & D; darker
 444 shades) represent the subsoil community composition.

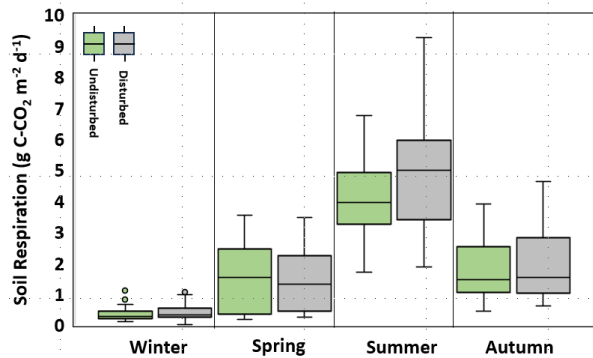
445 3.4 Soil Respiration

446 Total soil respiration rates showed distinct seasonal changes and were consistently higher, except
 447 during spring, at the disturbed site compared to the undisturbed one (Figure 9). The most significant
 448 activity occurred in the summer, with mean daily fluxes reaching $4.01 \pm 0.12 \text{ g C-CO}_2 \text{ m}^{-2} \text{ d}^{-1}$ at the
 449 undisturbed site and peaking at $4.81 \pm 0.17 \text{ g C-CO}_2 \text{ m}^{-2} \text{ d}^{-1}$ at the disturbed site, a statistically significant
 450 difference ($p < 0.0001$, ANOVA). Respiration rates declined in autumn, with mean daily fluxes of $1.79 \pm$
 451 $0.13 \text{ g C-CO}_2 \text{ m}^{-2} \text{ d}^{-1}$ (undisturbed) and $1.91 \pm 0.15 \text{ g C-CO}_2 \text{ m}^{-2} \text{ d}^{-1}$ (disturbed). The mean daily fluxes
 452 decreased further in spring, measuring $1.46 \pm 0.14 \text{ g C-CO}_2 \text{ m}^{-2} \text{ d}^{-1}$ (undisturbed) and $1.41 \pm 0.13 \text{ g C-CO}_2$
 453 $\text{m}^{-2} \text{ d}^{-1}$ (disturbed); during these two shoulder seasons, the differences between the sites were not
 454 statistically significant. The lowest mean daily efflux was recorded during winter, with rates dropping to
 455 $0.33 \pm 0.01 \text{ g C-CO}_2 \text{ m}^{-2} \text{ d}^{-1}$ at the undisturbed site and $0.39 \pm 0.13 \text{ g C-CO}_2 \text{ m}^{-2} \text{ d}^{-1}$ at the disturbed site,
 456 which, similar to the summer mean daily efflux, was also a statistically significant difference ($p < 0.01$,
 457 ANOVA). Annually, the disturbed site had a higher average soil efflux ($2.07 \pm 0.11 \text{ g C-CO}_2 \text{ m}^{-2} \text{ d}^{-1}$) than
 458 the undisturbed site ($1.81 \pm 0.09 \text{ g C-CO}_2 \text{ m}^{-2} \text{ d}^{-1}$), with the highest single mean daily flux of 9.27 g C-
 459 $\text{CO}_2 \text{ m}^{-2} \text{ d}^{-1}$ recorded on July 20 at the disturbed site.

460

Formatted: Font: Not Bold

461



462

463 **Figure 9.** Seasonal soil respiration patterns observed at the undisturbed and disturbed sites. Soil
464 respiration emissions are average **diel** fluxes from the 8 long-term chambers: 4 at undisturbed site
465 and 4 at disturbed site. The range of the boxplot represents the first and third quartiles, while the central
466 line signifies the median. The whiskers of the box extend to the minimum and maximum values, with
467 outliers represented by circles.

Formatted: Font: Not Bold

468

3.5 Linear regression analysis to determine important variables contributing to soil efflux

469

A linear regression analysis was performed on the mean daily averages to investigate the seasonal correlation between soil efflux and various factors, including air temperature, barometric pressure, seasonal thaw depth, topsoil and subsoil temperature, and volumetric water content (VWC) at both undisturbed and disturbed sites.

472

The analysis revealed that overall soil and air temperature exhibited the strongest correlation with soil

474

The analysis revealed that overall soil and air temperature exhibited the strongest correlation with

475

soil respiration across all sites during different seasons. Soil and air temperatures showed the strongest

476

correlations with soil efflux across all seasons. Seasonal R^2 values for soil temperatures ranged from

477

0.21–0.65 (winter), 0.87–0.92 (spring), 0.52–0.79 (summer), and 0.85–0.93 (autumn). Air temperature

478

also correlated strongly with soil efflux in spring ($R^2 = 0.74$ – 0.77) and autumn ($R^2 = 0.83$ – 0.87).

479

Moderate correlations were observed between soil efflux and thaw depth at both sites, with R^2 values

480

ranging from 0.39–0.50 in spring, 0.41–0.43 in summer, and 0.74 in autumn.

481

The correlation between soil efflux and topsoil and subsoil VWC varied during the summer and

482

fall seasons, as well as across the two soil layers. At the undisturbed site, in summer, moderate correlation

483

was found in the topsoil ($R^2 = 0.38$) and strong in the subsoil ($R^2 = 0.69$). In autumn, correlations were

484

strong in the topsoil ($R^2 = 0.62$) but weaker in the subsoil ($R^2 = 0.22$). At the disturbed site, in summer, the

485

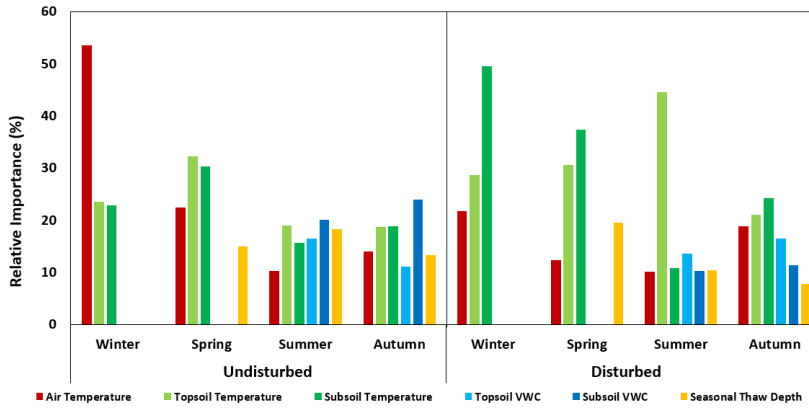
correlation was weak in the topsoil ($R^2 = 0.09$) but strong in the subsoil ($R^2 = 0.64$). In autumn, weak

486 correlations were observed in both layers ($R^2 = 0.28$ in topsoil and 0.10 in subsoil). Regression analysis
487 showed weak to no correlation between soil efflux and barometric pressure during winter and autumn (R^2
488 = 0.02–0.12) and no correlation in spring and summer. A slightly higher correlation was noted in winter
489 when using hourly averages ($R^2 = 0.23$ undisturbed, 0.18 disturbed).

490 3.6 Random forest efflux modeling

491 The non-linear RF model effectively captured the impact of disturbance on the variation in soil
492 respiration at both locations
493 , showing strong confidence levels with high R^2 and moderate to low mean
494 absolute error (MAE) values. Specifically, the model's R^2 values and corresponding MAE were 0.95 (0.14
495 MAE) for winter, 0.80 (0.38 MAE) for spring, 0.94 (0.16 MAE) for summer, and 0.82 (0.04 MAE) for
496 autumn at the undisturbed site, and 0.95 (0.12 MAE) for winter, 0.83 (0.52 MAE) for spring, 0.96 (0.13
497 MAE) for summer, and 0.84 (0.05 MAE) for autumn at the disturbed site. Skewness and kurtosis values
498 from the field data ranged from 0.04 - 1.24 and 1.61 - 4.56 at the disturbed site, and from 0.07 - 1.45 and
499 1.40 - 6.22 at the undisturbed site for all seasons, respectively. The ranges indicated that some instances
500 contained a more normal distribution while other instances, especially winter, were notably skewed and
501 tail-light and heavy.

502 The predictors' relative importance (RI) varied across seasons and sites (Figure 10). In the
503 winter model at the undisturbed site, air temperature emerged as the most influential predictor, accounting
504 for 53.6% RI. Conversely, at the disturbed site, the subsoil temperature exhibited the highest predictive
505 power with 49.6% RI (figure 10). For the spring model, soil temperature was the best predictor at both
506 sites, the topsoil layer temperature exhibited a slightly greater predictive power at the undisturbed site,
507 whereas the subsoil layer temperature proved to be more influential at the disturbed site. In the
508 undisturbed site's summer model, the soil moisture and temperature as well as the seasonal thaw depth
509 variables exhibit similar RI values, ranging from 15.7 to 20.2%. Among these variables, air temperature
510 has the lowest predictive power, with an RI of 10.3%. Conversely, at the disturbed site, the topsoil layer
511 temperature stands out as the strongest predictor, with an RI of 44.6%. It is followed by the topsoil VWC,
512 which has an RI of 13.7%. The undisturbed site's autumn model indicates that subsoil layer VWC has the
513 highest predictive power at 24.3% RI, followed by subsoil layer temperature at 18.9% RI, and topsoil
514 layer temperature at 18.7% RI. However, the disturbed autumn model shows that subsoil layer
515 temperature is the most influential factor in predicting CO₂ efflux with 24.3% RI and topsoil layer (21.1%
516 RI) and air (18.9% RI) also playing significant roles.



517

518 **Figure 10.** Relative importance (%) of variables to predict CO₂ efflux. Missing or static input variables
 519 (e.g. winter VWC and seasonal thaw depth) were not measured for importance.

Formatted: Font: Not Bold

520 Throughout the different seasons, various factors contribute to the varying degrees of relative
 521 importance regarding soil respiration. These factors include air temperature, the temperature of both
 522 topsoil and subsoil layers, and volumetric water content, which pertains only to subsoil. This information
 523 is presented in Table 1.

524 **Table 1.** Tabulation of the most important predictor variables to explain variability in the soil efflux data
 525 between disturbed and undisturbed sites as a function of season.

Formatted: Font: Not Bold

Season	Plot	Highest Predictor	RI
Winter	Undisturbed	Air temperature	53.6
Winter	Disturbed	Soil layer temperature (subsoil)	49.6
Spring	Undisturbed	Soil layer temperature (topsoil)	32.2
Spring	Disturbed	Soil layer temperature (subsoil)	37.4
Summer	Undisturbed	Volumetric water content (topsoil)	20.2
Summer	Disturbed	Soil layer temperature (topsoil)	44.6
Autumn	Undisturbed	Volumetric water content (subsoil)	24.0
Autumn	Disturbed	Soil layer temperature (subsoil)	24.3

526

527 **4. Discussion**

528 The primary objective of this study was to determine if an anthropogenic disturbance from
 529 approximately a century ago has a lasting legacy on carbon efflux in a boreal forest ecosystem. We

530 hypothesized that the disturbance would result in significant, persistent differences in soil respiration and
531 edaphic properties between the disturbed and an adjacent undisturbed site. Crucially, we extended this
532 hypothesis to the understudied winter period, postulating that these differences in soil activity would
533 persist even under extreme cold temperatures. To elucidate the controls behind these variations, we
534 examined seasonal CO₂ efflux alongside a suite of controlling factors, including soil temperature,
535 moisture, soil organic matter, pH, seasonal thaw depth, and microbial community composition. In the
536 following sections, we discuss how these interconnected variables explain the observed respiration
537 patterns, providing insight into the long-term trajectory of carbon cycling following historical disturbance
538 in permafrost environments.

539 Our findings show that the temperatures of the active layer soil were markedly elevated at the
540 disturbed site in comparison to the undisturbed site (Figure 3). Previous research, conducted in similar
541 subarctic environments, has attributed this increase in temperature, in disturbed
542 environments, to a decrease in insulating organic matter (Gordon *et al.*, 1987;
543 Amiro, 2001; Yoshikawa *et al.*, 2002; Koster *et al.*, 2017 and 2018; Zhu *et al.*, 2022
544) and alterations in surface albedo resulting from disturbance (Amiro, 2001; Yoshikawa *et al.*,
545 2002; Koster *et al.*, 2018; Zhu *et al.*, 2022). The consequences of the modified thermal conditions
546 were found to be significant, as the heightened soil temperatures
547 affected biogeochemical cycles (Chatterjee *et al.*, 2008; Akande *et al.*, 2023)
548 led to a deeper active layer (Forbes *et al.*,
549 2002; Foster *et al.*, 2022). In the current study, winter was the only season during
550 which soil temperatures were elevated at the undisturbed site (Figure 3), as
551 the unaltered surface vegetation provided a layer of insulation against the low air temperature. Snow did
552 not influence the thermal conditions at the study locations, as both sites were devoid of snow during the
553 winter to guarantee the proper functioning of the long-term chambers.

554 Disturbance had a significant impact on total carbon, total nitrogen (Figure 5), and soil pH in the
555 subsoil layer (SI Figure S5). In the subsoil, the average total carbon concentration at the disturbed site
556 was markedly higher than that at the undisturbed site (Figure 5). A comparable significant rise was noted
557 for total nitrogen in the subsoil of the disturbed site when contrasted with the undisturbed site (Figure 5).
558 Prior research has indicated that elevated carbon and nitrogen levels in the soil enhance soil respiration
559 (Oertel *et al.*, 2016, Akande *et al.*, 2023, Schepaschenko *et al.*, 2025). Nevertheless, in the topsoil layer,
560 these effects were not statistically significant, implying that the increase in soil respiration was likely
561 derived from the subsoil layer. Following this trend, soil pH in the subsoil was also significantly
562 impacted, with the mean pH in the disturbed site being significantly higher than the mean at the

Formatted: Subscript

563 undisturbed site.

564 Our results reveal a clear and persistent legacy of historical disturbance on soil carbon efflux,
565 with the disturbed site exhibiting significantly higher overall respiration rates than the adjacent
566 undisturbed site (Figure 9). This difference was most pronounced during the peak of the growing season,
567 where summer CO₂ fluxes at the disturbed site were nearly 20% higher, a statistically significant margin
568 ($p < 0.0001$). This finding strongly suggests that the initial disturbance—likely leading to warmer soils
569 and a deeper active layer—has created conditions that continue to favor more rapid decomposition a
570 century later. Interestingly, while respiration rates declined expectedly during the autumn and spring
571 shoulder seasons, the differences between the two sites became statistically insignificant. This may
572 indicate that during these transitional periods, other environmental factors, such as soil moisture levels)
573 or temperature thresholds, become more dominant controllers of microbial activity (Kim et al., 2012),
574 temporarily masking the underlying differences in soil properties. Crucially, our data demonstrate that the
575 elevated carbon loss at the disturbed site persists even into the winter. Although absolute fluxes were at
576 their lowest, the wintertime respiration at the disturbed site was still significantly higher than at the
577 undisturbed site ($p < 0.01$). This confirms that the ground remains a dynamic system and that the
578 historical disturbance has altered the soil's thermal regime or substrate availability in a way that sustains
579 higher microbial activity year-round, reinforcing the notion that winter is a critical (Natali et al., 2019;
580 Miner et al., 2022), and often overlooked, period for carbon cycling in these ecosystems.

581 Beyond the direct physical and chemical changes, the historical disturbance also left a significant
582 imprint on the soil's biological community The effects of disturbance on microbial community structure
583 were substantial, with significant alterations noted in both bacterial and fungal compositions (Figure
584 8). Notably, the date of sampling did not appear to influence community
585 structure, indicating that the disturbance itself serves as the principal factor driving these changes. This
586 finding is consistent with earlier studies that suggest soil disturbances can disrupt microbial habitats,
587 resulting in a reorganization of community dynamics (Chatterjee *et al.*, 2008; Dimitriu *et al.*, 2010). Such
588 changes can lead to cascading effects on ecosystem functions, including nutrient cycling and the
589 decomposition of organic matter (Peng *et al.*, 2008). We found that the disturbance-driven changes, led to
590 higher average soil temperatures and increased concentrations of mean SOM (LOI
591 (SI Figure S4), mean total carbon and mean total nitrogen
592 (Figure 5) in the subsoil which positively influenced the mean annual soil respiration rates, resulting
593 in an overall 14.4% increase when compared to the undisturbed site.

594 Our random forest model analysis found that key abiotic factors drive distinct seasonal patterns in
595 soil efflux between the disturbed and undisturbed sites (Figure 10)

Formatted: Subscript

596 . In winter, air temperature emerged as the most significant predictor for the undisturbed sites, likely due
597 to its direct impact on microbial activity and respiration rates. In contrast, the disturbed site during the
598 same season showed a stronger correlation with the subsoil layer temperature, suggesting that
599 disturbances may alter the thermal dynamics of the soil profile, making soil temperature a more crucial
600 determinant (Table 1). Moreover, given that both locations experienced snow denial, the more substantial
601 ground vegetation cover at the undisturbed site offered superior thermal insulation to the soil compared to
602 the thinner ground cover vegetation at the disturbed site. Furthermore, it is very likely that winter soil
603 respiration rates were higher at both sites where snow was not cleared, than at the chamber sites, as deep
604 snow can provide an insulating effect as found by Welker et al. (2000) and Miner et al. (2022). During
605 spring, topsoil layer temperature was the primary predictor for the undisturbed site, highlighting the
606 importance of organic matter decomposition driven by temperature changes. For the disturbed site, the
607 subsoil layer temperature remained the dominant factor, indicating that disturbances may have disrupted
608 the organic layer, shifting the focus to the subsoil layer's thermal conditions.

609 In the summer months, the volumetric water content in the subsoil layer emerged as the principal
610 predictor for the undisturbed site (Table 1), highlighting the essential role of moisture availability in
611 influencing microbial activity and respiration during this warmer period. Conversely, the disturbed site
612 exhibited a more pronounced correlation with the temperature of the topsoil layer (Table 1), indicating
613 that disturbances may have modified the soil's hydrological characteristics by increasing thaw depth and
614 enhancing drainage, which resulted in a reduced volumetric water content and rendered temperature a
615 more significant factor than moisture. As autumn approached, the volumetric water content in the subsoil
616 layer reestablished itself as the key predictor for the undisturbed site (Table 1), reaffirming the ongoing
617 significance of moisture for microbial functions as temperatures began to decline. In contrast, for the
618 disturbed site, the temperature of the subsoil layer continued to be the prevailing influence, underscoring
619 the enduring effects of disturbances on the thermal dynamics of the soil. Other permafrost study sites in
620 the Arctic have shown a reliance of soil efflux on soil moisture and temperature and suggest the
621 drying out of soil regimes and subsequent infiltration of snowmelt may also be a contributing factor for
622 predicting soil efflux values (Welker et al., 2000) and therefore annual data collection may likely be
623 necessary to determine long-term trends at sites where different soil types and disturbances exist.

624 Conclusion

625 Permafrost-affected ecosystems are experiencing dramatic change from anthropogenic causes,
626 both in terms of warming and physical disturbance to the soils. Active layers are deepening, unlocking
627 carbon that was previously inaccessible. Here, we sought to measure soil respiration in undisturbed and

628 [disturbed boreal forest sites to examine patterns of seasonality, the effect of legacy disturbance on soil](#)
629 [system, and the influence of soil abiotic properties on respiration. This is particularly timely because our](#)
630 [findings indicate that a historic disturbance in subarctic soils can have a lasting effect on the microbial](#)
631 [community composition, but less so on the seasonal activity of the soils. The discovery of persistent](#)
632 [microbial activity throughout the winter is critically significant, as future warming may prevent the active](#)
633 [layer from fully refreezing, thereby intensifying year-round decomposition and carbon release. There](#)
634 [were](#)
635 notable changes in soil temperature (162% warmer overall), the composition of bacterial communities
636 notable changes in soil temperature (162% warmer overall), the composition of bacterial communities
637 notable changes in soil temperature (162% warmer overall), the composition of bacterial communities
638 notable changes in
639 soil temperature (162% warmer overall), the composition of bacterial
640 communities (30% higher richness overall), total mean C (1% higher) and N (0.03%
641 higher) concentration levels and pH (11.9% higher) values in the subsoil layer, and the depth of the
642 maximum active thaw depth (147% deeper) as a result of disturbances, which subsequently led to
643 14.4% higher soil respiration rates. Soil respiration was primarily regulated by temperature, (air and soil)
644 while factors such as soil volumetric water content and the depth of the active layer also contributed, with
645 their relative importance varying throughout the different seasons. These findings underscore the complex
646 interplay between seasonal variations, long lasting effect of soil and vegetation disturbance, and abiotic
647 factors in determining soil respiration rates. Understanding these relationships is essential for accurate
648 modeling of carbon cycling and for developing effective strategies to mitigate the impacts of soil
649 disturbances on ecosystem functions. Both natural and anthropogenic disturbances can lead to a marked
650 rise in the emission of carbon dioxide and other greenhouse gases into the atmosphere. Neglecting to
651 account for these disturbances may result in a considerable underestimation of the role of soils in global
652 carbon cycles. Future investigations should concentrate on the long-term consequences of these dynamics,
653 especially considering ongoing warming change and its impact on permafrost regions.

654 *Data availability.* The datasets produced and/or examined in the present study can be obtained from the
655 corresponding author upon reasonable request.

656 *Author Contributions.* DAV conceptualized the study and managed the data collection, RAB provided
657 funding and insight on microbial data analysis, DAV, AJB, and WBB collected the soil samples, DAV and
658 DB performed the soil respiration analysis, JRW performed the soil property and microbial community
659 analyses. DAV drafted the initial manuscript and all authors contributed to revisions.

660 *Competing Interests.* The authors have no relevant financial or non-financial interests to disclose.

661 *Acknowledgements.* The authors express their gratitude to Ms. Elizabeth Corriveau for her work in
662 conducting quality assurance and quality control on the soil respiration time series data and to Ms. Anne
663 Katula for her efforts in processing the soil samples for analyses related to microbial composition and soil
664 properties.

665 *Financial support.* This work was founded by PE 0602144A Program Increase ‘Defense Resiliency
666 Platform Against Extreme Cold Weather’.

667 **References**

668 [Akande, O.J., Ma, Z., Huang, C., He, F. and Chang, S.X., 2023. Meta-analysis shows forest soil CO₂
669 effluxes are dependent on the disturbance regime and biome type. *Ecology Letters*, 26\(5\),
670 pp.765-777.](#)

671 Amiro, B.D., 2001. Paired-tower measurements of carbon and energy fluxes following disturbance in the
672 boreal forest. *Global Change Biology*, 7(3), pp.253-268.

673 Anderson, M.J., 2001. A new method for non-parametric multivariate analysis of variance. *Austral
674 ecology*, 26(1), pp.32-46.

675 Apprill, A., McNally, S., Parsons, R. and Weber, L., 2015. Minor revision to V4 region SSU rRNA 806R
676 gene primer greatly increases detection of SAR11 bacterioplankton. *Aquatic Microbial Ecology*,
677 75(2), pp.129-137.

678 Baker, C.C.M., Barker, A.J., Douglas, T.A., Doherty, S.J. and Barbato, R.A. 2023 Seasonal variation in
679 near-surface seasonally thawed active layer and permafrost soil microbial communities *Environ
680 Res Lett* **18** 055001

681 Barbato, R.A., Jones, R.M., Douglas, T.A., Doherty, S.J., Messan, K., Foley, K.L., Perkins, E.J., Thurston,
682 A.K. and Garcia-Reyero, N., 2022. Not all permafrost microbiomes are created equal: Influence
683 of permafrost thaw on the soil microbiome in a laboratory incubation study. *Soil Biology and
684 Biochemistry*, 167, p.108605.

685 Behnamian, A., Millard, K., Banks, S.N., White, L., Richardson, M. and Pasher, J., 2017. A systematic
686 approach for variable selection with random forests: achieving stable variable importance values.
687 *IEEE Geoscience and Remote Sensing Letters*, 14(11), pp.1988-1992.

688 Bonan, G.B., 2008. Forests and climate change: forcings, feedbacks, and the climate benefits of
689 forests. *science*, 320(5882), pp.1444-1449.

690 Bond-Lamberty, B., Bailey, V.L., Chen, M., Gough, C.M. and Vargas, R., 2018. Globally rising soil
691 heterotrophic respiration over recent decades. *Nature*, 560(7716), pp.80-83.

692 Bray, J.R. and Curtis, J.T., 1957. An ordination of the upland forest communities of southern
693 Wisconsin. *Ecological monographs*, 27(4), pp.326-349.

694 Callahan, B.J., McMurdie, P.J., Rosen, M.J., Han, A.W., Johnson, A.J.A. and Dada, S.H., High-resolution
695 sample inference from Illumina amplicon data., 2016, 13. DOI: [https://doi.org/10.1038/nmeth, 3869](https://doi.org/10.1038/nmeth.3869), pp.581-583.

696

697 Caporaso, J.G., Lauber, C.L., Walters, W.A., Berg-Lyons, D., Lozupone, C.A., Turnbaugh, P.J., Fierer, N.
698 and Knight, R., 2011. Global patterns of 16S rRNA diversity at a depth of millions of sequences
699 per sample. *Proceedings of the national academy of sciences*, 108(supplement_1), pp.4516-4522.

700 Caporaso, J.G., Lauber, C.L., Walters, W.A., Berg-Lyons, D., Huntley, J., Fierer, N., Owens, S.M., Betley,
701 J., Fraser, L., Bauer, M. and Gormley, N., 2012. Ultra-high-throughput microbial community
702 analysis on the Illumina HiSeq and MiSeq platforms. *The ISME journal*, 6(8), pp.1621-1624.

703 Chatterjee, A., Vance, G.F., Pendall, E. and Stahl, P.D., 2008. Timber harvesting alters soil carbon
704 mineralization and microbial community structure in coniferous forests. *Soil Biology and*
705 *Biochemistry*, 40(7), pp.1901-1907.

706 Chi, J., Zhao, P., Klosterhalfen, A., Jocher, G., Kljun, N., Nilsson, M.B. and Peichl, M., 2021. Forest floor
707 fluxes drive differences in the carbon balance of contrasting boreal forest stands. *Agricultural and*
708 *Forest Meteorology*, 306, p.108454.

709 [Dimitriu, P.A. and Grayston, S.J., 2010. Relationship between soil properties and patterns of bacterial \$\beta\$ -](#)
710 [diversity across reclaimed and natural boreal forest soils. *Microbial ecology*, 59\(3\), pp.563-573.](#)

711 [Doherty, S.J., Barbato, R.A., Grandy, A.S., Thomas, W.K., Monteux, S., Dorrepaal, E., Johansson, M. and](#)
712 [Ernakovich, J.G., 2020. The transition from stochastic to deterministic bacterial community](#)
713 [assembly during permafrost thaw succession. *Frontiers in Microbiology*, 11, p.596589.](#)

714 Fekete, I., Kotroczó, Z., Varga, C., Nagy, P.T., Várбірó, G., Bowden, R.D., Tóth, J.A. and Lajtha, K.,
715 2014. Alterations in forest detritus inputs influence soil carbon concentration and soil respiration
716 in a Central-European deciduous forest. *Soil Biology and Biochemistry*, 74, pp.106-114.

- 717 [Forbes, B.C., Ebersole, J.J. and Strandberg, B., 2001. Anthropogenic disturbance and patch dynamics in](#)
718 [circumpolar arctic ecosystems. *Conservation biology*, 15\(4\), pp.954-969.](#)
- 719 [Foster, A.C., Wang, J.A., Frost, G.V., Davidson, S.J., Hoy, E., Turner, K.W., Sonnentag, O., Epstein, H.,](#)
720 [Bernier, L.T., Armstrong, A.H. and Kang, M., 2022. Disturbances in North American boreal forest](#)
721 [and Arctic tundra: impacts, interactions, and responses. *Environmental Research Letters*, 17\(11\),](#)
722 [p.113001.](#)
- 723 Gordon, A.M., Schlentner, R.E. and Cleve, K.V., 1987. Seasonal patterns of soil respiration and CO₂
724 evolution following harvesting in the white spruce forests of interior Alaska. *Canadian Journal of*
725 *Forest Research*, 17(4), pp.304-310.
- 726 Grace, J., 2004. Understanding and managing the global carbon cycle. *Journal of Ecology*, 92(2), pp.189-
727 202.
- 728 Harel, A., Sylvain, J.D., Drolet, G., Thiffault, E., Thiffault, N. and Tremblay, S., 2023. Fine scale
729 assessment of seasonal, intra-seasonal and spatial dynamics of soil CO₂ effluxes over a balsam
730 fir-dominated perhumid boreal landscape. *Agricultural and Forest Meteorology*, 335, p.109469.
- 731 Jorgenson, M.T., Douglas, T.A., Liljedahl, A.K., Roth, J.E., Cater, T.C., Davis, W.A., Frost, G.V., Miller,
732 P.F. and Racine, C.H., 2020. The roles of climate extremes, ecological succession, and hydrology
733 in repeated permafrost aggradation and degradation in fens on the Tanana Flats, Alaska. *Journal*
734 *of Geophysical Research: Biogeosciences*, 125(12), p.e2020JG005824.
- 735 [Kim, Y., Kimball, J.S., Zhang, K. and McDonald, K.C., 2012. Satellite detection of increasing Northern](#)
736 [Hemisphere non-frozen seasons from 1979 to 2008: Implications for regional vegetation growth.](#)
737 [Remote Sensing of Environment, 121, pp.472-487.](#)
- 738 Kõljalg, U., Nilsson, R.H., Abarenkov, K., Tedersoo, L., Taylor, A.F., Bahram, M., Bates, S.T., Bruns,
739 T.D., Bengtsson-Palme, J., Callaghan, T.M. and Douglas, B., 2013. Towards a unified paradigm
740 for sequence-based identification of fungi.
- 741 Köster, E., Köster, K., Berninger, F., Aaltonen, H., Zhou, X. and Pumpanen, J., 2017. Carbon dioxide,
742 methane and nitrous oxide fluxes from a fire chronosequence in subarctic boreal forests of
743 Canada. *Science of the Total Environment*, 601, pp.895-905.
- 744 Köster, E., Köster, K., Berninger, F., Prokushkin, A., Aaltonen, H., Zhou, X. and Pumpanen, J., 2018.
745 Changes in fluxes of carbon dioxide and methane caused by fire in Siberian boreal forest with
746 continuous permafrost. *Journal of environmental management*, 228, pp.405-415.

747 Lei, Q., Yu, H. and Lin, Z., 2024. Understanding China's CO2 emission drivers: Insights from random
748 forest analysis and remote sensing data. *Heliyon*, 10(7).

749 Martin, B.D., Witten, D. and Willis, A.D., 2021. Corncob: count regression for correlated observations
750 with the beta-binomial.

751 Marty, C., Piquette, J., Morin, H., Bussi eres, D., Thiffault, N., Houle, D., Bradley, R.L., Simpson, M.J.,
752 Ouimet, R. and Par e, M.C., 2019. Nine years of in situ soil warming and topography impact the
753 temperature sensitivity and basal respiration rate of the forest floor in a Canadian boreal
754 forest. *PLoS One*, 14(12), p.e0226909.

755 [Miner, K.R., Turetsky, M.R., Malina, E., Bartsch, A., Tamminen, J., McGuire, A.D., Fix, A., Sweeney, C.,
756 Elder, C.D. and Miller, C.E., 2022. Permafrost carbon emissions in a changing Arctic. *Nature
757 Reviews Earth & Environment*, 3\(1\), pp.55-67.](#)

758 M older, F., Jablonski, K.P., Letcher, B., Hall, M.B., Tomkins-Tinch, C.H., Sochat, V., Forster, J., Lee, S.,
759 Twardziok, S.O., Kanitz, A., Wilm, A., Holtgrewe, M., Rahmann, S., Nahnsen, S., and K oster, J.
760 (2021). Sustainable data analysis with Snakemake. **F1000Research** 10:33.
761 doi:10.12688/f1000research.29032.1

762 [Natali, S.M., Watts, J.D., Rogers, B.M., Potter, S., Ludwig, S.M., Selbmann, A.K., Sullivan, P.F., Abbott,
763 B.W., Arndt, K.A., Birch, L. and Bj orkman, M.P., 2019. Large loss of CO2 in winter observed
764 across the northern permafrost region. *Nature climate change*, 9\(11\), pp.852-857.](#)

765 Nilsson, R.H., Larsson, K.H., Taylor, A.F.S., Bengtsson-Palme, J., Jeppesen, T.S., Schigel, D., Kennedy,
766 P., Picard, K., Gl ockner, F.O., Tedersoo, L. and Saar, I., 2019. The UNITE database for molecular
767 identification of fungi: handling dark taxa and parallel taxonomic classifications. *Nucleic acids
768 research*, 47(D1), pp.D259-D264.

769 [Oertel, C., Matschullat, J., Zurba, K., Zimmermann, F. and Erasmi, S., 2016. Greenhouse gas emissions
770 from soils—A review. *Geochemistry*, 76\(3\), pp.327-352.](#)

771 Oksanen J, Simpson G, Blanchet F, Kindt R, Legendre P, Minchin P, O'Hara R, Solymos P, Stevens M,
772 Szoecs E, Wagner H, Barbour M, Bedward M, Bolker B, Borcard D, Carvalho G, Chirico M, De
773 Caceres M, Durand S, Evangelista H, FitzJohn R, Friendly M, Furneaux B, Hannigan G, Hill M,
774 Lahti L, McGlenn D, Ouellette M, Ribeiro Cunha E, Smith T, Stier A, Ter Braak C, Weedon J
775 (2024). *_vegan: Community Ecology Package_*. R package version 2.6-6.1, <[https://CRAN.R-
776 project.org/package=vegan](https://CRAN.R-project.org/package=vegan)>.

777 Pan, Y., Birdsey, R.A., Fang, J., Houghton, R., Kauppi, P.E., Kurz, W.A., Phillips, O.L., Shvidenko, A.,
778 Lewis, S.L., Canadell, J.G. and Ciais, P., 2011. A large and persistent carbon sink in the world's
779 forests. *science*, 333(6045), pp.988-993.

780 Parada, A.E., Needham, D.M. and Fuhrman, J.A., 2016. Every base matters: assessing small subunit
781 rRNA primers for marine microbiomes with mock communities, time series and global field
782 samples. *Environmental microbiology*, 18(5), pp.1403-1414.

783 Parker, T.C., Clemmensen, K.E., Friggens, N.L., Hartley, I.P., Johnson, D., Lindahl, B.D., Olofsson, J.,
784 Siewert, M.B., Street, L.E., Subke, J.A. and Wookey, P.A., 2020. Rhizosphere allocation by
785 canopy-forming species dominates soil CO₂ efflux in a subarctic landscape. *New*
786 *Phytologist*, 227(6), pp.1818-1830.

787 [Peng, Y., Thomas, S.C. and Tian, D., 2008. Forest management and soil respiration: Implications for](#)
788 [carbon sequestration. *Environmental Reviews*, 16\(NA\), pp.93-111.](#)

789 Quast, C., Pruesse, E., Yilmaz, P., Gerken, J., Schweer, T., Yarza, P., Peplies, J. and Glöckner, F.O., 2012.
790 The SILVA ribosomal RNA gene database project: improved data processing and web-based
791 tools. *Nucleic acids research*, 41(D1), pp.D590-D596.

792 R-Core-Team, 2018. R: A Language and Environment for Statistical Computing, R Foundation for
793 Statistical Computing.

794 Rodtassana, C., Unawong, W., Yaemphum, S., Chanthorn, W., Chawchai, S., Nathalang, A., Brockelman,
795 W.Y. and Tor-ngern, P., 2021. Different responses of soil respiration to environmental factors
796 across forest stages in a Southeast Asian forest. *Ecology and Evolution*, 11(21), pp.15430-15443.

797 [Schepaschenko, D., Mukhortova, L. and Shvidenko, A., 2025. Estimation of Impact of Disturbances on](#)
798 [Soil Respiration in Forest Ecosystems of Russia. *Forests*, 16\(6\), p.925.](#)

799 Schonlau, M. and Zou, R.Y., 2020. The random forest algorithm for statistical learning. *The Stata Journal*,
800 20(1), pp.3-29.

801 [Shiklomanov, N.I., Streletskiy, D.A., Little, J.D. and Nelson, F.E., 2013. Isotropic thaw subsidence in](#)
802 [undisturbed permafrost landscapes. *Geophysical Research Letters*, 40\(24\), pp.6356-6361.](#)

803 Smith, D.P. and Peay, K.G., 2014. Sequence depth, not PCR replication, improves ecological inference
804 from next generation DNA sequencing. *PLoS one*, 9(2), p.e90234.

805 Soil Survey Staff. 2022. Keys to Soil Taxonomy, 13th edition. USDA Natural Resources Conservation
806 Service

- 807 Storer, D.A., 1984. A simple high sample volume ashing procedure for determination of soil organic
808 matter. *Communications in Soil Science and plant analysis*, 15(7), pp.759-772.
- 809 Turetsky, M.R., Abbott, B.W., Jones, M.C., Anthony, K.W., Olefeldt, D., Schuur, E.A., Grosse, G., Kuhry,
810 P., Hugelius, G., Koven, C. and Lawrence, D.M., 2020. Carbon release through abrupt permafrost
811 thaw. *Nature Geoscience*, 13(2), pp.138-143.
- 812 [Vas, D.A., Corriveau, E.J., Gaimaro, L.W. and Barbato, R.A., 2023. Challenges and Limitations of Using
813 Autonomous Instrumentation for Measuring In Situ Soil Respiration in a Subarctic Boreal Forest
814 in Alaska, USA.](#)
- 815 Walters, W., Hyde, E.R., Berg-Lyons, D., Ackermann, G., Humphrey, G., Parada, A., Gilbert, J.A.,
816 Jansson, J.K., Caporaso, J.G., Fuhrman, J.A. and Apprill, A., 2016. Improved bacterial 16S rRNA
817 gene (V4 and V4-5) and fungal internal transcribed spacer marker gene primers for microbial
818 community surveys. *Msystems*, 1(1), pp.10-1128.
- 819 Watts, J.D., Natali, S.M., Minions, C., Risk, D., Arndt, K., Zona, D., Euskirchen, E.S., Rocha, A.V.,
820 Sonnentag, O., Helbig, M. and Kalhori, A., 2021. Soil respiration strongly offsets carbon uptake
821 in Alaska and Northwest Canada. *Environmental Research Letters*, 16(8), p.084051.
- 822 [Welker, J.M., Fahnestock, J.T. and Jones, M.H., 2000. Annual CO2 Flux in Dry and Moist Arctic Tundra:
823 Field Responses to Increases in Summer Temperatures and Winter Snow Depth. *Climatic
824 Change*. 44, 139-150.](#)
- 825 West, J.R., Whitman, T., 2022. Disturbance by soil mixing decreases microbial richness and supports
826 homogenizing community assembly processes. *FEMS Microbiology Ecology*, 98, 1–11.
- 827 Wickham, H. and Wickham, H., 2016. *Data analysis* (pp. 189-201). Springer International Publishing.
- 828 Willis, A., Bunge, J. and Whitman, T., 2017. Improved detection of changes in species richness in high
829 diversity microbial communities. *Journal of the Royal Statistical Society Series C: Applied
830 Statistics*, 66(5), pp.963-977.
- 831 Yilmaz, P., Parfrey, L.W., Yarza, P., Gerken, J., Pruesse, E., Quast, C., Schweer, T., Peplies, J., Ludwig, W.
832 and Glöckner, F.O., 2014. All-species Living Tree Project (LTP) taxonomic frameworks. *Nucleic
833 Acids Res*, 42, pp.D643-D648.
- 834 [Yoshikawa, K., Bolton, W.R., Romanovsky, V.E., Fukuda, M. and Hinzman, L.D., 2002. Impacts of wildfire
835 on the permafrost in the boreal forests of Interior Alaska. *Journal of Geophysical Research:
836 Atmospheres*, 107\(D1\), pp.FFR-4.](#)

837 [Zhu, X., Xu, X. and Jia, G., 2023. Recent massive expansion of wildfire and its impact on active layer](#)
838 [over pan-Arctic permafrost. Environmental Research Letters, 18\(8\), p.084010.](#)